

Visualizing High-Dimensional Temporal Data Using Direction-Aware t-SNE

Pavlin G. Poličar^{1*} and Blaž Zupan^{1,2}

^{1*}Faculty of Computer and Information Science, University of Ljubljana,
Večna Pot 113, Ljubljana, 1000, Slovenia.

²Department of Education, Innovation and Technology, Baylor College
of Medicine, 1 Baylor Plz, Houston, 77030, Texas, United States.

*Corresponding author(s). E-mail(s): pavlin.policar@fri.uni-lj.si;

Abstract

Many real-world data sets contain a temporal component or involve transitions from state to state. For exploratory data analysis, we can represent these high-dimensional data sets in two-dimensional maps, using embeddings of the data objects under exploration and representing their temporal relationships with directed edges. Most existing dimensionality reduction techniques, such as t-SNE and UMAP, do not take into account the temporal or relational nature of the data when constructing the embeddings, resulting in temporally cluttered visualizations that obscure potentially interesting patterns. To address this problem, we propose two complementary, direction-aware loss terms in the optimization function of t-SNE that emphasize the temporal aspects of the data, guiding the optimization and the resulting embedding to reveal temporal patterns that might otherwise go unnoticed. The Directional Coherence Loss (DCL) encourages nearby arrows connecting two adjacent time series points to point in the same direction, while the Edge Length Loss (ELL) penalizes arrows - which effectively represent time gaps in the visualized embedding - based on their length. Both loss terms are differentiable and can be easily incorporated into existing dimensionality reduction techniques. By promoting local directionality of the directed edges, our procedure produces more temporally meaningful and less cluttered visualizations. We demonstrate the effectiveness of our approach on a toy dataset and two real-world datasets.

Keywords: Temporal-data visualization, Dimensionality reduction, Data visualization

1 Introduction

A common approach to analyzing the structure of high-dimensional data involves representing it in two-dimensional, point-based visualizations. We can use dimensionality reduction approaches such as principal component analysis, multi-dimensional scaling, or t-distributed stochastic neighbor embedding to obtain such data maps. Additionally, we can indicate temporal relations between data points by overlaying these data maps with arrows. This depiction has been used extensively for the visualization of dynamic graphs [1], multi-variate time-series [2], linguistic analysis [3], and bioinformatics [4].

Existing approaches to visualize temporal data via two-dimensional embeddings rely primarily on standard embedding techniques that do not take into account the temporal aspects of the data. However, commonly used dimensionality reduction approaches may be semantically limited. For example, principal component analysis (PCA) [5] relies on the linear transformation of attribute space and may fail to reveal complex patterns with non-linear interactions of input features. Nonlinear data embedding techniques, such as multidimensional scaling [6], t-distributed stochastic neighbor embedding (t-SNE) [7], and uniform manifold approximation and projection (UMAP) [8], overcome this limitation but introduce distortions into the embedding. However, none of these techniques can incorporate temporal information into the embedding. When such information is available – the real life data most often includes measurements that change with time – the resulting embeddings and their visualizations would fail to reflect, or even obscure, the temporal patterns in the underlying data.

This report introduces two novel loss terms, the *directional coherence loss* (DCL) and the *edge length loss* (ELL), which address the available temporal information and integrate it into the embedding construction process. The DCL and ELL are differentiable and can be incorporated into existing dimensionality reduction techniques. We integrate them into the t-SNE dimensionality reduction algorithm and refer to the resulting approach as *Direction-Aware t-SNE* (DA-t-SNE). The resulting embeddings are designed to facilitate the discovery of temporal patterns in the two-dimensional embedding space. Incorporating directional awareness into existing dimensionality reduction approaches reveals temporal patterns in the resulting embeddings, thus facilitating the discovery of temporal patterns in the data.

2 Related Work

There are a variety of approaches we can use to visualize high-dimensional, temporal data. Rauber *et al.* [9] developed Dynamic t-SNE, which constructs a series of t-SNE embeddings and stacks them along a third dimension corresponding to time. A similar approach has been proposed for UMAP, called AlignedUMAP [8]. While attractive, Sedlmair *et al.* [10] showed that three-dimensional embeddings offer little advantage over two-dimensional embeddings in terms of perception, but typically require interactive tools for effective navigation. Therefore, static two-dimensional embeddings are often “good enough”.

Alternatively, van den Elzen *et al.* [1] portray the progression of time in two-dimensional embeddings by connecting data points with arrows. Their approach

focuses on visualizing dynamic graphs. At each point in time, the graph adjacency matrix is treated as a high-dimensional data point. This high-dimensional collection of graph snapshots is subsequently embedded into a two-dimensional visualization using an off-the-shelf embedding technique. Ali *et al.* [2] apply a similar approach to multivariate time-series data, where each sliding time window is treated as a single high-dimensional data point. In this way, they embed temporal sequences into two dimensions, where arrows connect consecutive time points. Unlike dynamic t-SNE and AlignedUMAP, which construct a three-dimensional embedding by stacking multiple two-dimensional embeddings along a time dimension, these approaches illustrate the entire temporal progression into two dimensions and indicate dependence using arrows.

In bioinformatics, single-cell RNA velocity [4] may accompany more standard gene expression data and requires a different visualization approach. Each data point corresponds to the gene expression of a single cell, characterized by tens of thousands of genes. Then, for each cell, single-cell RNA velocity estimates the likely transitions between different cell states, for instance, during differentiation. The resulting visualization typically consists of a two-dimensional embedding constructed using t-SNE or UMAP overlaid with arrows to indicate likely cell-to-cell transitions. This approach is conceptually similar to van den Elzen *et al.* [1] and Ali *et al.* [2], where we deal only with a single time step for every cell.

Another notable approach, Time Curves [11], offers general guidelines for visualizing the temporal progression of a single entity. The framework may be viewed as a generalization of the work by Ali *et al.* [2], allowing for arbitrary time steps between snapshots.

3 Methods

Consider a high-dimensional data set $\mathbf{X} \in \mathbb{R}^{N \times d}$, where N is the number of data points and d is the dimensionality of each data point. Let G be a directed graph $G = (V, E)$, where V denotes the set of vertices v_i corresponding to individual data points \mathbf{x}_i . E is the set of edges e_{ij} representing the temporal connections between data points i and j . When visualizing high-dimensional data sets, our primary objective is to find a low-dimensional embedding $\mathbf{Y} \in \mathbb{R}^{N \times 2}$ that accurately reflects the topological features of \mathbf{X} . In two-dimensional visualizations, we represent the connections e_{ij} as directed line segments \mathbf{p}_{ij} (depicted as arrows) linking two related data points i and j in the embedding space such that $\mathbf{p}_{ij} = [\mathbf{y}_i, \mathbf{y}_j]$.

3.1 t-SNE

t -distributed stochastic neighbor embedding (t-SNE) is a non-linear dimensionality reduction technique commonly used to visualize high-dimensional data [7]. t-SNE aims to find a low-dimensional representation \mathbf{Y} such that if two data points are close in the high-dimensional space \mathbf{X} , then they are also close in the low-dimensional space \mathbf{Y} .

Formally, the t-SNE algorithm aims to find a low-dimensional representation \mathbf{Y}^* , such that the Kullback-Leibler (KL) divergence $D_{\text{KL}}(\mathbf{P} \parallel \mathbf{Q})$ between similarities \mathbf{P} between pairs of data points in the high-dimensional space \mathbf{X} and the similarities \mathbf{Q}

between pairs of data points in the low-dimensional space \mathbf{Y} is minimized, such that

$$\mathbf{Y}^* = \arg \min_{\mathbf{Y}} \text{KL}(\mathbf{P} \parallel \mathbf{Q}). \quad (1)$$

The similarities $\mathbf{P} = [p_{ij}]$ between data points in \mathbf{X} are obtained using the Gaussian kernel,

$$p_{ij} = \frac{p_{j|i} + p_{i|j}}{2N}, \quad p_{j|i} = \frac{\exp(-\mathcal{D}(\mathbf{x}_i, \mathbf{x}_j)/2\sigma_i^2)}{\sum_{k \neq i} \exp(-\mathcal{D}(\mathbf{x}_i, \mathbf{x}_k)/2\sigma_i^2)}, \quad p_{i|i} = 0, \quad (2)$$

where \mathcal{D} is some distance measure and the bandwidth of each Gaussian kernel σ_i is selected such that the perplexity u of each conditional distribution $p_{i|j}$ matches a user-specified parameter value,

$$\log(u) = -\sum_j p_{j|i} \log(p_{j|i}) \quad (3)$$

In the low-dimensional space \mathbf{Y} , the similarities $\mathbf{Q} = [q_{ij}]$ are characterized by the t-distribution,

$$q_{ij} = \frac{(1 + \|\mathbf{y}_i - \mathbf{y}_j\|^2)^{-1}}{\sum_{k \neq i} (1 + \|\mathbf{y}_k - \mathbf{y}_i\|^2)^{-1}}, \quad q_{ii} = 0. \quad (4)$$

3.2 Direction-Aware Losses (DAL)

We here introduce two loss functions that, when included into existing dimensionality reduction approaches, produce temporally more meaningful, low-dimensional embeddings. To encourage the formation of smooth temporal patterns in the embedding space, the *Directional Coherence Loss* (DCL) [12] ensures that nearby arrows point in similar directions. Complementing the DCL, we introduce the *Edge Length Loss* (ELL), which penalizes long arrows. These two losses work in tandem to produce more temporally consistent visualizations. We bundle the two loss functions into a single loss, which we refer to as the *Direction-Aware Loss* (DAL).

3.2.1 Directional Coherence Loss (DCL)

The key idea behind the *Directional Coherence Loss* (DCL) [12] is that arrows close to one another in the low-dimensional embedding space \mathbf{Y} should point in approximately the same direction. Since each arrow is defined as a line segment parameterized by points \mathbf{y}_i and \mathbf{y}_j , we can achieve directional coherence by adjusting the positions of points \mathbf{y}_i and \mathbf{y}_j accordingly.

Let \mathbf{u}_{ij} be the unit vector corresponding to the line segment $\mathbf{p}_{ij} = [\mathbf{y}_i, \mathbf{y}_j]$,

$$\mathbf{u}_{ij} = \mathbf{p}_{ij} / \|\mathbf{p}_{ij}\|, \quad \mathbf{p}_{ij} = \mathbf{y}_j - \mathbf{y}_i. \quad (5)$$

For each pair of edges e_{ij} and e_{kl} in E , we can determine the directional coherence of their corresponding arrows in the embedding by computing the dot product $\mathbf{u}_{ij} \cdot \mathbf{u}_{kl} =$

$\|\mathbf{u}_{ij}\| \|\mathbf{u}_{kl}\| \cos \theta$, where θ denotes the angle between the two vectors. In our case, $\|\mathbf{u}_{ij}\| = \|\mathbf{u}_{kl}\| = 1$, so their dot product simplifies to $\mathbf{u}_{ij} \cdot \mathbf{u}_{kl} = \cos \theta$. When \mathbf{u}_{ij} and \mathbf{u}_{kl} point in the same direction, their dot product is 1. Conversely, when \mathbf{u}_{ij} and \mathbf{u}_{kl} point in opposite directions, their dot product is -1 . Therefore, to achieve good directional coherence for any pair of arrows in E , we must maximize the dot product of their corresponding directional vectors.

To make our notion of directional coherence compatible with existing dimensionality reduction approaches, we convert the directional coherence into a strictly positive minimization loss. To convert the maximization into a minimization objective, we multiply the equation with -1 . To enforce strict-positivity and avoid negative penalties, we add a $+1$ term to the above formulation and shift the domain from $[-1, 1]$ to $[0, 2]$. Additionally, we have found it beneficial to square the resulting equation, leading to faster convergence and more visually appealing visualizations. The directional coherence loss between edges pair of edges e_{ij} and e_{kl} then becomes

$$\text{DCL}(\mathbf{p}_{ij}, \mathbf{p}_{kl}) = (- (\mathbf{u}_{ij} \cdot \mathbf{u}_{kl}) + 1)^2 \quad (6)$$

Applying the DCL to all pairs of arrows would force all arrows to point in the same direction, regardless of their proximity in the embedding space. Instead, we want only nearby arrow pairs to point in the same direction, therefore, we penalize only nearby arrow pairs. The distance between two line segments $\mathbf{p}_{ij} = [\mathbf{y}_i, \mathbf{y}_j]$ and $\mathbf{p}_{kl} = [\mathbf{y}_k, \mathbf{y}_l]$ is defined as

$$d(\mathbf{p}_{ij}, \mathbf{p}_{kl}) = \arg \min_{s,t} \| [s \cdot \mathbf{y}_i + (1-s) \cdot \mathbf{y}_j] - [t \cdot \mathbf{y}_k + (1-t) \cdot \mathbf{y}_l] \|, \quad (7)$$

where $s, t \in [0, 1]$. Intuitively, the distance between two line segments corresponds to the distance between the two closest points on these line segments. If the line segments intersect, then their distance is 0.

We penalize nearby arrow pairs using a Gaussian kernel on the obtained pairwise line-segment distances,

$$w(\mathbf{p}_{ij}, \mathbf{p}_{kl}) = \frac{1}{\sqrt{2\pi\sigma^2}} \exp(-d(\mathbf{p}_{ij}, \mathbf{p}_{kl})/2\sigma^2), \quad (8)$$

where σ^2 is the variance of the Gaussian distribution. The variance σ^2 determines the region around each arrow where we wish the arrows to point in the same direction. This parameter can greatly affect the final embedding, as a large value of σ^2 will enforce the DCL across the entire embedding. In contrast, small values of σ^2 will have a limited effect on the point positions. It is also worth noting that this parameter should depend on the scale of the embeddings, which can change during optimization and vary across different dimensionality reduction algorithms.

Combining the directionality penalty from Eqn. 6 and the weights from Eqn. 8, we obtain the final directional coherence loss,

$$\mathcal{L}_{DCL} = \frac{1}{\binom{|E|}{2}} \sum_{e_{ij} \in E} \sum_{e_{kl} \in E} w(\mathbf{p}_{ij}, \mathbf{p}_{kl}) (-(\mathbf{u}_{ij} \cdot \mathbf{u}_{kl}) + 1)^2, \quad (i, j) \neq (k, l). \quad (9)$$

3.2.2 Edge Length Loss (ELL)

Another important factor to consider when drawing arrows is the length of the arrows. Longer arrows that span the embedding space are more likely to cross other arrows, cluttering the visualization. In addition, note that arrows connect the data points that are immediate neighbors of their respective time sequences, and we want them to be close together in the embedding space. To encourage the formation of shorter arrows, we introduce the *Edge Length Loss* (ELL), which penalizes arrow lengths,

$$\mathcal{L}_{ELL} = \frac{1}{|E|} \sum_{e_{ij} \in E} \|\mathbf{p}_{ij}\|^\alpha. \quad (10)$$

Here, the exponent α is a user-specified length modulation parameter that dictates to what degree longer arrows should be penalized over shorter ones. The effects of this parameter are discussed in more detail in Section 5.2.

3.3 Optimization

We can incorporate both proposed loss function into various dimensionality reduction methods. In this work, we incorporate the proposed direction aware (DA) losses into the t-SNE algorithm, which we refer to as Direction-Aware t-SNE (DA-t-SNE). The resulting DA-t-SNE loss is a combination of the three loss terms,

$$\mathcal{L}_{DA-t-SNE} = \mathcal{L}_{t-SNE} + \lambda_{DCL} \mathcal{L}_{DCL} + \lambda_{ELL} \mathcal{L}_{ELL}, \quad (11)$$

where λ_{DCL} and λ_{ELL} denote the penalty strength for the DCL and ELL, respectively.

Following the conventions of standard t-SNE, the optimization procedure consists of two phases. During the first *early exaggeration* phase, the attractive forces between data points are increased by some factor ρ , typically set to 12 [7]. This allows the points to move more freely in the embedding to find their respective neighbors. In the second phase of the optimization, the attractive forces are reset to their original values with $\rho = 1$. We apply DCL and ELL uniformly throughout both optimization phases. We perform the optimization with batch gradient descent using the delta-bar-delta update rule [13] and using the learning rate N/ρ as proposed by Belkina *et al.* [14].

Including these loss terms, especially the DCL, empirically results in slower convergence and typically requires more iterations to reach a stable minimum. Therefore, we run the optimization for 10,000 iterations in all of our experiments, as opposed to the typical 750 iterations, as is standard in modern t-SNE implementations [15].

4 Case Studies

We demonstrate the conceptual idea and the expected results of our approach in three case studies. The first one uses a synthetic toy dataset. We then apply our approach to two real-world data sets, highlighting the progression of the COVID-19 pandemic in Slovenia and the evolution of the semantic meanings of words over time.

4.1 Toy Example

We use a toy example to demonstrate that adding the DCL to the t-SNE dimensionality reduction algorithm reveals trajectories or transitions between different clusters. This synthetic dataset consists of seven distinct, non-overlapping clusters, equally spaced, each containing 50 points sampled from unit Gaussian distributions. To simulate transitions between clusters, we connect each point from a given cluster c to a randomly chosen point from the next cluster $c + 1$. The data points in the last cluster of a sequence of connected clusters are connected back to the data points in the first cluster. This toy example can be thought of as a cyclic process with seven different states, where transitions are only possible between adjacent states. For example, this may correspond to single cell data containing gene expression profiles corresponding to four different cell cycle states in cell division.

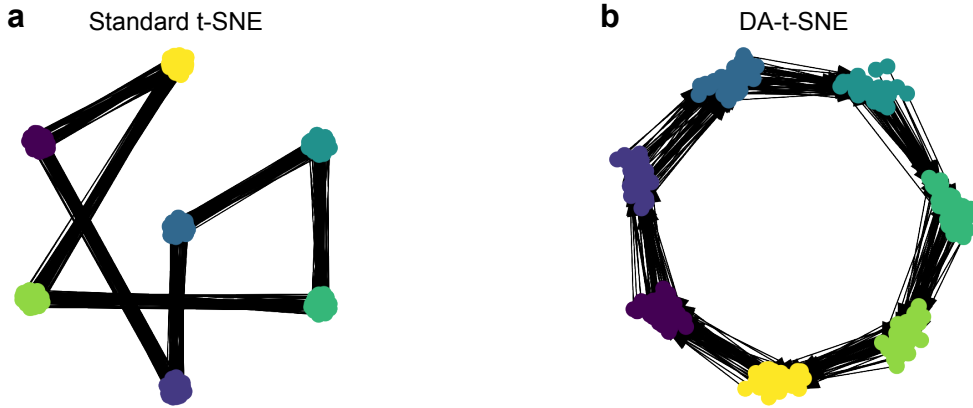


Fig. 1 The toy example shows that incorporating the directional coherence loss (DCL) can help highlight the temporal transitions between data points. We construct a standard t-SNE embedding in (a), which can recover the seven distinct clusters. However, the arrows between clusters cross over one another, making it challenging to infer the underlying cyclic pattern. Incorporating the DCL in (b) helps untangle the crossing arrows and highlights the cyclic pattern in the underlying data set while still recovering the seven clusters.

Fig. 1.a shows that while t-SNE can recover the seven distinct clusters from the high-dimensional space, overlaying the embedding with arrows clutters the visualization, concealing the cyclic pattern in the underlying data set. On the other hand, augmenting the standard t-SNE loss function with the DCL untangles the arrows and

highlights the cyclic pattern as shown in Fig. 1.b. Combining the t-SNE dimensionality reduction algorithm, which can identify the distinct clusters, with the DCL, which positions the clusters so that the transitions between the clusters are most apparent, greatly improves the interpretability of the embedding and the underlying temporal pattern.

The t-SNE algorithm aims to preserve distances to a user-specified number of neighbors. However, accurately preserving distances obtained from high-dimensional data sets in a two-dimensional embedding is only possible in some of the most straightforward data sets. Using a perplexity value of 30, t-SNE does its best to preserve distances to each point’s 30 nearest neighbors in the high-dimensional space. However, t-SNE also attempts to preserve distances to other data points, albeit to a much lesser extent. In our synthetic data set, each cluster comprises 50 data points, meaning that, in addition to the points in the same cluster, t-SNE also attempts to preserve at least some distances from the other clusters.

In Fig. 1.a, the purple cluster is positioned centrally to other clusters, roughly at equal distances from the remaining clusters. Here, t-SNE can preserve the distances reasonably well. On the other hand, the top-left yellow cluster appears close to the central purple cluster and the light-green cluster below it, suggesting that these clusters are closer to one another than to, for instance, the right-most green cluster. However, by design, all seven clusters are at equal distances from one another in the high-dimensional space and cannot be accurately embedded in a two-dimensional plane. Consequently, the between-cluster distances in all nearest-neighbor-based two-dimensional embeddings are often meaningless and should never be taken at face value. This is a general limitation of dimensionality reduction techniques and has been documented in numerous reviews, e.g., by Nonato and Aupetit [16].

Note, however, that incorporating the DAL necessarily reduces the embedding quality with respect to the t-SNE loss function. For instance, although the distances between clusters were poorly preserved in Fig. 1.a, the between-cluster distance distortions were arguably less severe than in Fig. 1.b, where each cluster is closest to its preceding and subsequent cluster, and progressively further from the remainder. This layout indicates that adjacent clusters are more similar than non-adjacent ones when, in reality and disregarding the temporal constraints, all clusters are at equal distances from one another. Nonetheless, despite this embedding being quantitatively worse at preserving distances between clusters, we argue that it provides a more informative visualization. When constructing embeddings for high-dimensional data sets, distances between clusters in the embedding should never be taken at face value, regardless of the dimensionality reduction technique. While the spatial relationships between clusters can aid in hypothesis generation, they should always be validated using alternative techniques.

Given that the spatial relationships between clusters lack informative value and can even mislead, it would be more sensible to position clusters in a temporally coherent manner. In this way, at least, the temporal relationships are more clearly highlighted, and the user is more directly aware of the limitations of interpreting spatial relationships, an often overlooked limitation of non-linear dimensionality methods. This way, the embedding algorithm can still recover well-defined clusters of data points in the

high-dimensional space. Still, we explicitly decide that the spatial positions will reflect the temporal component of the embedding and not the spatial relationships between clusters.

4.2 COVID-19 Pandemic in Slovenia

We obtained Slovenian national data on the COVID-19 pandemic spanning from the beginning of March 2020 up until the end of March 2022¹. Although the data includes many variables, for illustrative purposes, we limit our analysis to three time-series variables: the daily number of tests performed, the daily number of confirmed cases, and the daily number of hospitalized patients. We plot the individual time series in Fig. 2.a. The line plots indicate the progression of the COVID-19 pandemic in Slovenia, with visible distinct phases of the pandemic.

To construct a two-dimensional visualization of the pandemic progression through time, we follow the approach from Ali *et al.* [2]. We first convert this multi-variate time series into a high-dimensional data set by constructing vectors with a sliding window of size 7. Thus, each of the 160 21-dimensional data points represents one week of the pandemic. We connect data points corresponding to subsequent weeks with arrows.

We construct a t-SNE visualization of the high-dimensional data set in Fig. 2.b. While the plot shows a clear progression through time, it does not reveal any underlying patterns in the data. Fig. 2.c shows the results of our approach. While the embedding has not changed much structurally, the visualization reveals two clear cyclic patterns in the upper right and lower regions of the embedding space.

Let us investigate the top-left cyclic pattern in Fig. 2.c. Inspecting the two corresponding time spans highlighted in the original time series in Fig. 2.a, it appears that this cyclic pattern coincides with high hospitalization rates, moderate levels of testing, and a moderate number of positive tests. Interestingly, both periods occurred during the spring season, one in 2021 and one in 2022. The first of these periods was substantially longer, lasting to the end of May, while the second lasted only a month and a half. It is also interesting to inspect which COVID-19 variants were prevalent in the country at that time². During the first period in 2021, we were dealing with the initial 20A strain. The second period coincides with the transition from the Delta strain to the Omicron strain. The highlighted region in Fig. 2.a corresponds to the final weeks of the Delta variant, which had higher mortality rates than the Omicron variant [17]. These strain prevalence and dynamics may explain the subsequent peak in the positive test cases and lower hospitalization rate following the highlighted region.

Finally, the incorporation of DAL into the t-SNE algorithm elucidates the temporal evolution of the time series. For example, in Figs. 2.e and 2.e, we focus on a particular region of the embedding space where it initially appears that the standard t-SNE embedding highlights the temporal progression better than with the addition of the DAL. Upon closer inspection, however, it is difficult to follow the arrows indicating the temporal progression of the pandemic, as the arrow seems to veer off to the right, then cycle back, only to make another cycle back to the starting point. It is unclear

¹National Slovenian data on the COVID-19 pandemic is available at <https://covid-19.sledilnik.org/en/stats>.

²The prevalence of the different COVID-19 variants in different countries is available at <https://covariants.org/per-country>

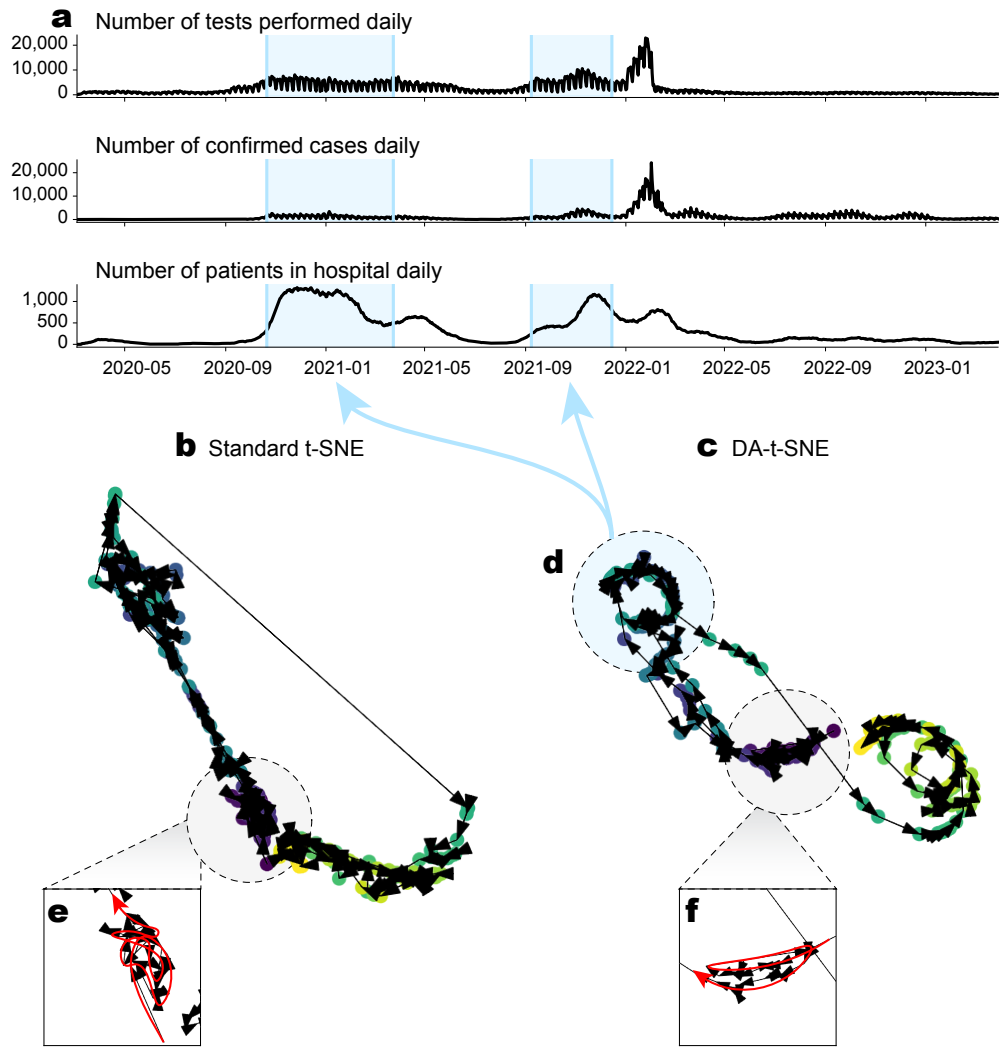


Fig. 2 The progression of the COVID-19 pandemic in Slovenia from March 2020 to March 2022. (a) depicts individual line plots of the three variables under consideration. We construct a t-SNE embedding of the multivariate time series in (b) and augment the t-SNE loss function with our directional coherence loss in (c). Individual points correspond to one week of the time series. We indicate the chronological progression by point colors where dark, purple colors correspond to the start of the pandemic, while lighter, yellow colors coincide with later stages of the pandemic. We connect consecutive weeks by arrows. Incorporating the directional coherence loss uncovers interesting temporal patterns in the visualization. We highlight one such cyclic region in (d) and mark the corresponding time spans in the original line plots. Panels (e) and (f) provide close-up views of regions of the original and augmented t-SNE embedding. We clarify the time progression by superimposing a red arrow onto the plot.

which of these cycles occurred first and which second. With the addition of the DAL,

it becomes easy to follow the temporal progression, as indicated by the red arrow drawn on top of the arrows to make the embedding easier to read.

4.3 Temporal Word Embeddings

Hamilton *et al.* [3] study the changes in the semantic meaning of words over time. In their study, the authors develop an approach for obtaining diachronic word embeddings that map a given word w into a vector representation \mathbf{z}_w^t at time t . This way, separate embedding vectors can be obtained for each word at different time points, enabling us to study how the embeddings associated with a single word change over time.

One striking example from the study illustrates how the meaning of the word “gay” changed throughout the 20th century. In the early 20th century, the word was typically associated with sweetness, cheeryness, and wittyness. However, its meaning gradually changed, and the word became associated with homosexuality by the end of the century.

Here, we replicate Hamilton *et al.*’s findings by constructing a t-SNE embedding augmented with our DAL approach. We obtain the “English Fiction” variants of the pre-trained word2vec [18] embeddings³. A temporal embedding is available for each word at several discrete time points t , where $t \in T; T = \{1800, 1810, \dots, 1980, 1990\}$. Some words are very uncommon in the earlier years and are mapped into a constant embedding vector.

In their visualization approach, Hamilton *et al.* first identify the k nearest neighbor words of a particular word of interest w at all time points T . Then, using only these nearest neighbor words, they construct a reference t-SNE embedding using their most recent temporal embeddings $\mathbf{z}_w^{|T|}$. Next, to embed the word of interest w into the embedding space, they obtain word embeddings \mathbf{z}_w^t at all time points $t \in T$ and add these to the reference embedding. The reference embedding is kept fixed while the point positions corresponding to word w are obtained via direct optimization.

While effective for showing the evolution of single words, Hamilton *et al.*’s approach has several drawbacks. Firstly, it focuses on the changes of a single word. Instead, it may be interesting to observe how the meaning of multiple words or groups of words changes over time. Secondly, as noted by Poličar *et al.* [19], optimizing out-of-sample data points in this fashion will necessarily position them near points in the reference embedding, regardless of whether or not these representations are actually similar to their nearest neighbors or not. Ideally, out-of-sample points, which are not similar to any points in the reference embedding, would be placed away from samples in the reference embedding. It may be thus interesting to embed multiple words’ temporal embeddings into a joint embedding space.

We plot the results of our analysis in Fig. 3. We note that because of the quadratic scaling of the DCL, the embedding includes only 38 words, which are highlighted in the original study. Figs. 3.a and c show the embeddings obtained from original t-SNE and DA-t-SNE, respectively. In both embeddings, the bottom cluster corresponds to samples mapped to constant vectors by the diachronic embedding procedure and should be disregarded. In Fig. 3.b, we overlay the trajectory of the evolution of the

³Diachronic word2vec embeddings are available at <https://nlp.stanford.edu/projects/histwords/>.

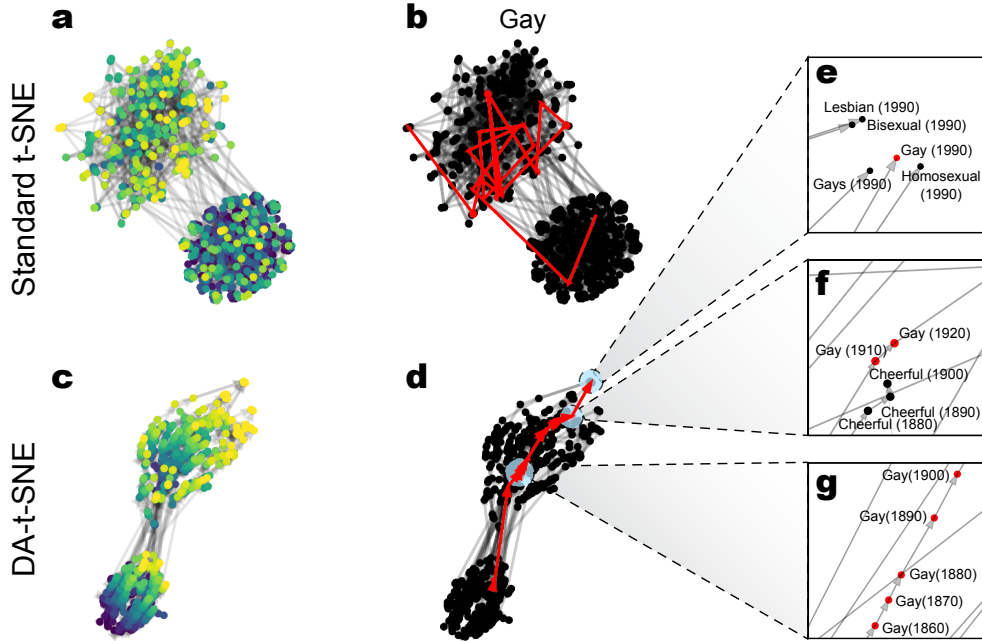


Fig. 3 The plot of the evolution of the semantic meaning of words through time. Hamilton *et al.* [3] construct diachronic word2vec embeddings for each word of interest. We embed these words into two dimensions using standard t-SNE in (a). As before, we indicate the chronological progression by point colors where dark, purple colors correspond to the beginning and the lighter, yellow colors correspond to the ending of the time sequence. In their publication, Hamilton *et al.* demonstrate how the meaning of the word “gay” changed through the 20th century. Likewise, we plot the trajectory of the “gay” through the t-SNE embedding in (b). Because standard t-SNE does not consider the temporal nature of the data, the trajectory jumps between multiple regions of the embedding space, resulting in an incoherent trajectory. We construct a t-SNE embedding augmented with the DAL in (c) and depict the trajectory of the word “gay” in (d), which shows a more smooth and coherent trajectory throughout the embedding space. We plot several interesting regions through which the word passes through in (e), (f), and (g).

word “gay” onto the embedding produced by standard t-SNE. Since t-SNE does not account for the temporal nature of the data, the trajectory resembles a wild tangle of arrows with no clear direction or pattern. On the other hand, incorporating our direction-aware loss in Fig. 3.d produces a clear trajectory throughout the embedding space, which we can trace from the bottom of the embedding to the top.

Inspecting the regions of the embedding space through which the word trajectory passes, we can draw similar conclusions as Hamilton *et al.* [3]. Fig. 3.e shows the most recent embeddings from 1990 that show that the word “gay” was associated with homosexuality. Moving backward along the trajectory, we observe in Fig. 3.f that the word had a similar semantic meaning as “cheerful” at the beginning of the 20th century. Going further back still reveals limited insight, as the word embeddings follow a relatively consistent straight line, with no notable neighboring words.

5 Discussion

Incorporating the direction-aware loss terms introduces four new user parameters, each of which can have a marked impact on the resulting embedding. The DCL introduces two parameters, λ_{DCL} and σ , which affect the strength and scale at which the DCL is enforced. The ELL also introduces two parameters, λ_{ELL} and α , which specify the strength and modulation of the penalizing arrow lengths. Enforcing these losses may conflict with the point placement prioritized by the t-SNE loss function. Therefore, care must be taken when choosing parameter values to achieve a balanced visualization. Optimal parameters are likely to vary from dataset to dataset. To understand the impact of each of these parameter values, we will examine their effects on the resulting visualizations in more detail.

5.1 Effects of DCL Scale

In our prior work [12], we applied a single, fixed scale parameter σ to the DCL throughout the optimization. However, this fails to account for a range of embedding scales that embeddings typically undergo throughout optimization. For instance, a typical t-SNE embedding is initialized so that its variance is equal to 0.0001. Throughout optimization, embeddings expand and often end up with scales between 10 and 100. Using this configuration, the DCL will be applied uniformly across all data samples during the early stages of optimization, when the embedding occupies a small, dense region of the space. As the embedding expands, the DCL is applied ever more locally until its effect on the global directional coherence is negligible.

Therefore, applying a single, fixed scale parameter value to the DCL fails to account for the expanding nature of the embedding throughout the optimization. Instead, we here use an adaptive scale parameter, specified as a fraction of the entire embedding span, calculated at each iteration of the optimization. Next, we investigate the effects of different scale parameter values. To isolate the effects of scale, we hold the remaining parameters constant, using $\lambda_{\text{DCL}} = 10$ and disable the ELL loss, setting $\lambda_{\text{ELL}} = 0$.

Fig. 4 shows the effects of increasing the scale parameter σ on the resulting embedding. Lower values of σ reveal more local temporal patterns, while larger values tend to enforce directional coherence along the entire embedding, often resulting in a qualitatively worse embedding. For instance, the cyclical toy data set in Fig. 4.a shows that the cycle is recovered when using lower scales but is distorted when increasing the scale to cover the entire span of the embedding. Fig. 4.b shows the results of the COVID-19 data set. Small scales nicely reveal the smaller cycles, which get gradually hidden as we increase the scale parameter. Fig. 4.c shows the results on the word meaning data sets, where, again, local patterns are revealed at smaller scales. In this case, any visible patterns disappear already when setting the scale to 0.1.

5.2 Effects of ELL modulation

We next investigate the role of the length modulation parameter α in the ELL loss. This parameter modulates to what extent and in what way the length of arrows in the embedding are penalized. For smaller values of $0 < \alpha < 1$, longer arrows are penalized less severely than shorter arrows relative to their lengths. This allows longer arrows

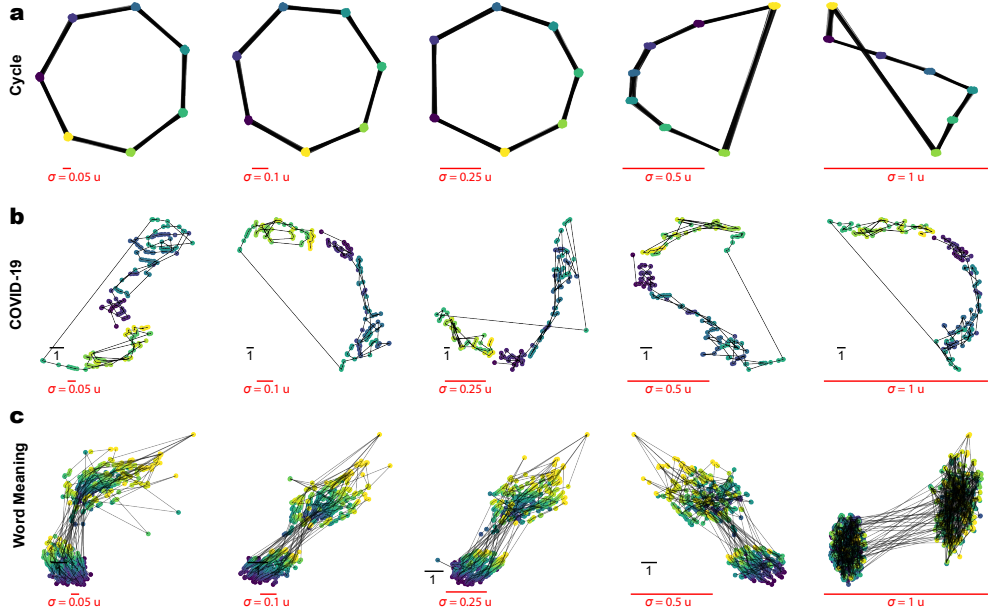


Fig. 4 The effect of the scale parameter σ in the DCL. We show the scale σ using a red bar, showing the effective range of the DCL.

to connect different regions of the embedding space. Larger values of $1 < \alpha$ instead penalize longer arrows more severely, and shorter arrows are preferred. To isolate its effects on the resulting visualizations, we hold the remaining parameters constant, using $\lambda_{\text{DCL}} = 10$, $\lambda_{\text{ELL}} = 0.5$, and scale $\sigma = 0.05$.

Fig. 5 shows the effect of increasing the ELL parameter α on the three data sets. Lower values of α distribute errors across different error lengths more uniformly, resulting in qualitatively more diverse lengths of arrows. As we increase α , we progressively increase the penalization of longer arrows. This penalization has two visible effects on the final visualization. First, since arrow lengths are dependent on the positions of the points in the two-dimensional space, points will be positioned closer to one another, effectively reducing the scale of the embedding. This is especially apparent in Fig. 5.a where increasing α has little effect on the cyclical structure but compresses the embedding, as indicated by the black scale bars. This likely counterweights the t-SNE loss function, in which repulsive forces prevent points from being placed too close to one another. Second, since longer arrows are penalized, arrows connecting different regions of the embedding space are less likely to occur. For instance, for low values of α in Fig. 5.b, several longer arrows traverse the embedding space, connecting disjoint clusters. However, as we increase α , these long arrows disappear, and points are forced to be spaced more evenly along a given trajectory. A similar effect is also visible in Fig. 5.c. This effect is also reflected in the distribution of arrow lengths, as shown below each visualization in Fig. 5. Increasing α generally reduces the average length of the arrows.

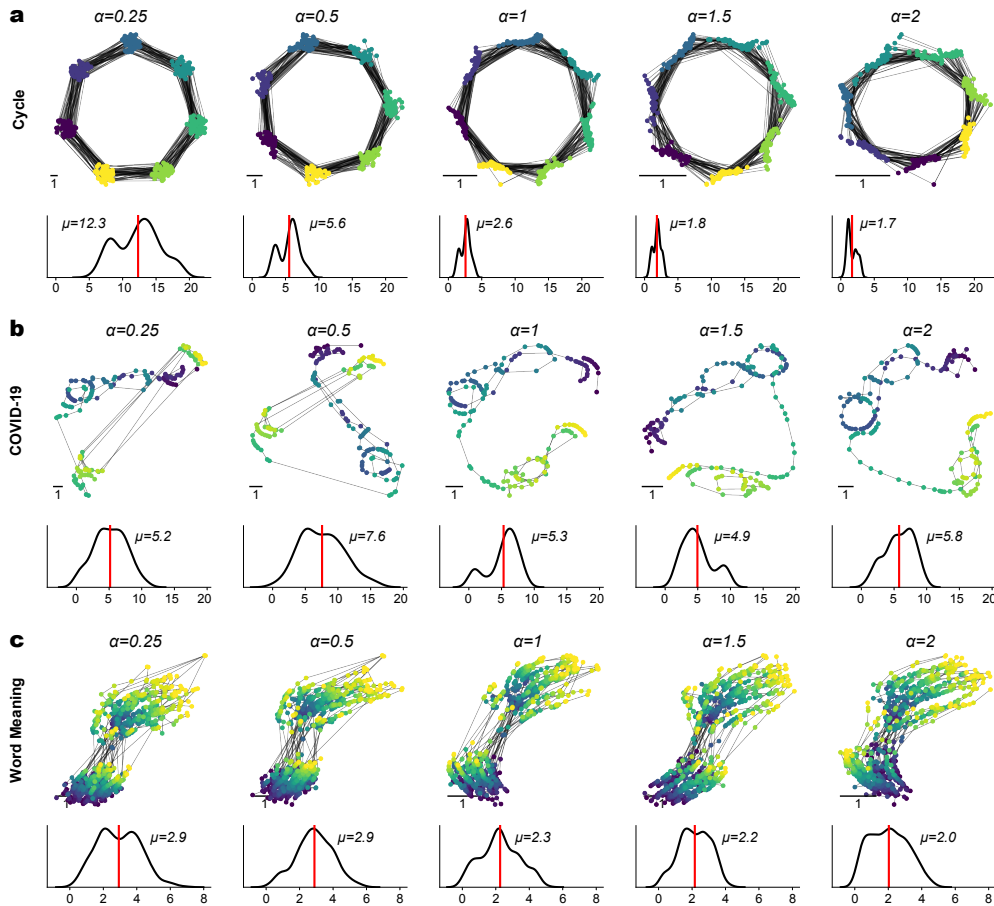


Fig. 5 The effect of different values of the α parameter in the ELL. Underneath each two-dimensional embedding, we show the corresponding distribution of arrow lengths. We also indicate the scale of the embedding with black bars showing the width of a unit vector in the embedding space.

5.3 On the Interplay between the DCL and ELL

The previous sections have focused on the individual parameters of the DCL and ELL in isolation. In practice, however, different combinations of their parameter settings and penalty strengths result in markedly different visualizations. We demonstrate this interplay on a range of penalty strength combinations in Fig. 6. To isolate the effects of penalty strengths, we hold the remaining parameters constant, using length modulation $\alpha = 1.5$ and scale $\sigma = 0.05$.

Fig. 6.a shows the standard t-SNE embedding. As discussed previously, this plot reveals only one overarching trajectory from the bottom-right to the top-left sections of the plot. Increasing the DCL penalty via λ_{DCL} enforces more directional coherence, which begins to reveal cycles in Fig. 6.b, that become even more pronounced in Fig. 6.c. However, enforcing such a strong DCL compromises the low-dimensional structure

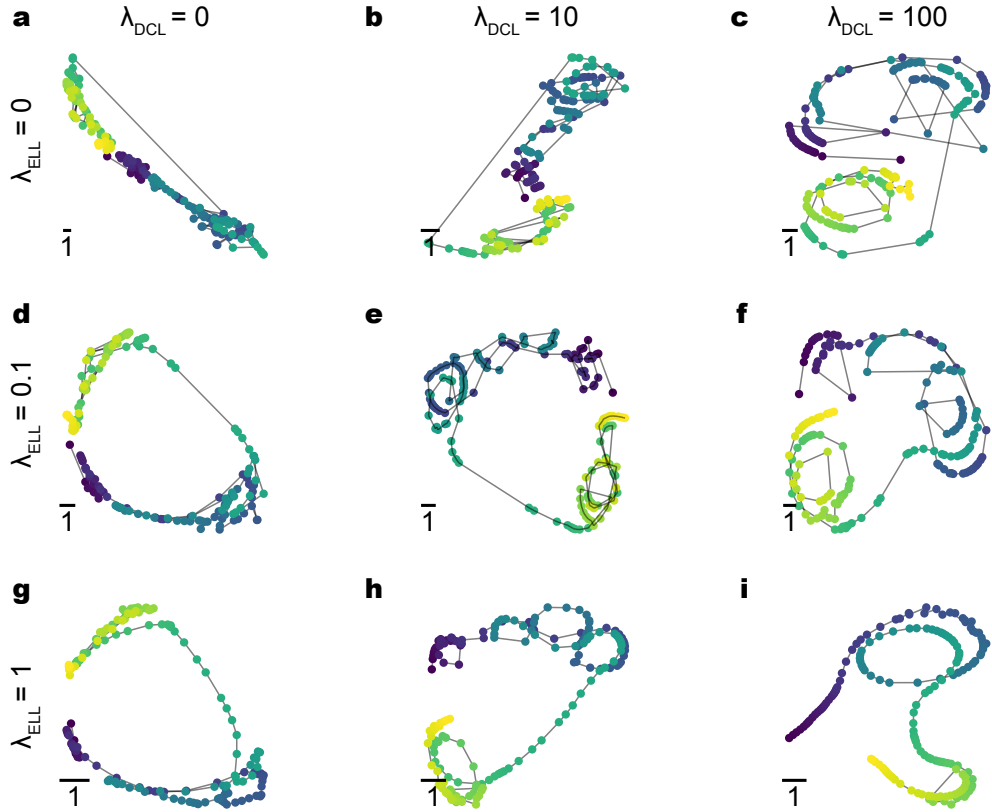


Fig. 6 The interplay between different strengths of the DCL and ELL terms.

found by t-SNE. Instead of increasing the DCL penalty, we can instead increase the ELL penalty in tandem, which forces arrows to be shorter. Empirically, this seems to preserve the original t-SNE topology better than the DCL alone, while still clearly revealing the temporal patterns. For instance, Fig. 6.e begins to show the two cycles in this particular data set. Increasing the ELL penalty further enforces shorter arrows, distributing the points more evenly along the trajectory. Of course, increasing both penalties further leads to a very clear temporal structure, but becomes quite far from the original t-SNE topology.

6 Conclusion

Our reported work was motivated by the difficulty of identifying temporal patterns in the representation of multivariate data in low-dimensional, nonlinear embeddings. In such cases, the temporal relationships can be revealed by using arrows to indicate state transitions over time. These new visualization elements often clutter data displays and obscure the underlying temporal patterns. Existing dimensionality reduction techniques do not account for the temporal nature of the data. To this end, we propose two

direction-aware loss (DAL) terms, comprising of the *directional coherence loss* (DCL) and the *edge length loss*. These can be readily incorporated into existing dimensionality reduction techniques such as t-SNE or UMAP. Uniquely, these losses explicitly integrate temporal information into the embedding construction process and produce embeddings that more clearly highlight the temporal patterns in the underlying data.

This presented work opens up several avenues for future research. First, the DAL enforces directional coherence by affecting the positions of the data points in the two-dimensional embedding. While this approach is viable for simpler data sets, such an arrangement may be difficult to achieve in the presence of more complex patterns. Secondly, the DAL exhibits quadratic scaling in the number of connections between data points, making it unsuitable for the visualization of large data sets. Modern implementations of popular non-linear dimensionality reduction may address data sets containing up to millions of data points [8, 15]. In its current form, the DAL scales with quadratic time complexity, allowing it to be applied to data sets containing at most several thousands of data points. Developing more efficient implementation and approximation schemes would enable the approach outlined in this manuscript to be applied to larger data sets. Due to the local nature of the DAL, approximation schemes could be developed which would only compute the interaction between nearby line segments.

Funding. This work was supported by the Slovenian Research Agency Program Grant P2-0209 and Project Grant V2-2272.

Conflict of Interest. The authors report no conflict of interest.

Author Contribution. P.G.P. developed the approach and ran experiments. P.G.P. and B.Z. wrote and reviewed the manuscript.

References

- [1] Elzen, S., Holten, D., Blaas, J., Wijk, J.J.: Reducing Snapshots to Points: A Visual Analytics Approach to Dynamic Network Exploration. *IEEE Transactions on Visualization and Computer Graphics* **22**(1), 1–10 (2016) <https://doi.org/10.1109/TVCG.2015.2468078>
- [2] Ali, M., Jones, M., Xie, X., Williams, M.: Towards Visual Exploration of Large Temporal Datasets. In: 2018 International Symposium on Big Data Visual and Immersive Analytics (BDVA), pp. 1–9 (2018). <https://doi.org/10.1109/BDVA.2018.8534025>
- [3] Hamilton, W.L., Leskovec, J., Jurafsky, D.: Diachronic word embeddings reveal statistical laws of semantic change. In: Erk, K., Smith, N.A. (eds.) *Proceedings of the 54th Annual Meeting of the Association for Computational Linguistics (Volume 1: Long Papers)*, pp. 1489–1501. Association for Computational Linguistics, Berlin, Germany (2016). <https://doi.org/10.18653/v1/P16-1141>
- [4] La Manno, G., Soldatov, R., Zeisel, A., Braun, E., Hochgerner, H., Petukhov, V., Lidschreiber, K., Kastrioti, M.E., Lönnerberg, P., Furlan, A., Fan, J., Borm, L.E.,

- Liu, Z., Bruggen, D., Guo, J., He, X., Barker, R., Sundström, E., Castelo-Branco, G., Cramer, P., Adameyko, I., Linnarsson, S., Kharchenko, P.V.: RNA velocity of single cells. *Nature* **560**(7719), 494–498 (2018) <https://doi.org/10.1038/s41586-018-0414-6>
- [5] Jolliffe, I.T.: *Principal Component Analysis*. Springer, New York (2002). <https://doi.org/10.1007/b98835>
- [6] Kruskal, J.B., Wish, M.: *Multidimensional Scaling*. SAGE Publications, Inc., London (1978). <https://doi.org/10.4135/9781412985130>
- [7] Maaten, L., Hinton, G.: Visualizing data using t-SNE. *Journal of Machine Learning Research* **9**(Nov), 2579–2605 (2008)
- [8] McInnes, L., Healy, J., Melville, J.: UMAP: Uniform Manifold Approximation and Projection for Dimension Reduction. *ArXiv e-prints* (2018) [arXiv:1802.03426](https://arxiv.org/abs/1802.03426) [stat.ML]
- [9] Rauber, P.E., Falcão, A.X., Telea, A.C.: Visualizing time-dependent data using dynamic t-SNE. In: *EuroVis 2016 - Short Papers*, pp. 73–77. The Eurographics Association, Groningen, the Netherlands (2016). <https://doi.org/10.2312/eurovisshort.20161164>
- [10] Sedlmair, M., Munzner, T., Tory, M.: Empirical guidance on scatterplot and dimension reduction technique choices. *IEEE Transactions on Visualization and Computer Graphics* **19**(12), 2634–2643 (2013) <https://doi.org/10.1109/TVCG.2013.153>
- [11] Bach, B., Shi, C., Heulot, N., Madhyastha, T., Grabowski, T., Dragicevic, P.: Time Curves: Folding Time to Visualize Patterns of Temporal Evolution in Data. *IEEE Transactions on Visualization and Computer Graphics* **22**(1), 559–568 (2016) <https://doi.org/10.1109/TVCG.2015.2467851>
- [12] Poličar, P.G., Zupan, B.: Refining temporal visualizations using the directional coherence loss. In: Bifet, A., Lorena, A.C., Ribeiro, R.P., Gama, J., Abreu, P.H. (eds.) *Discovery Science*, pp. 204–215. Springer, Cham (2023). https://doi.org/10.1007/978-3-031-45275-8_14
- [13] Jacobs, R.A.: Increased rates of convergence through learning rate adaptation. *Neural Networks* **1**(4), 295–307 (1988)
- [14] Belkina, A.C., Ciccolella, C.O., Anno, R., Halpert, R., Spidlen, J., Snyder-Cappione, J.E.: Automated optimized parameters for t-distributed stochastic neighbor embedding improve visualization and analysis of large datasets. *Nature Communications* **10**(1), 1–12 (2019)
- [15] Poličar, P.G., Stražar, M., Zupan, B.: openTSNE: a modular Python library for

t-SNE dimensionality reduction and embedding. *BioRxiv*, 731877 (2019)

- [16] Nonato, L.G., Aupetit, M.: Multidimensional projection for visual analytics: Linking techniques with distortions, tasks, and layout enrichment. *IEEE Transactions on Visualization and Computer Graphics* **25**(8), 2650–2673 (2019)
- [17] Wrenn, J.O., Pakala, S.B., Vestal, G., Shilts, M.H., Brown, H.M., Bowen, S.M., Strickland, B.A., Williams, T., Mallal, S.A., Jones, I.D., *et al.*: COVID-19 severity from Omicron and Delta SARS-CoV-2 variants. *Influenza and Other Respiratory Viruses* **16**(5), 832–836 (2022) <https://doi.org/10.1111/irv.12982>
- [18] Mikolov, T., Chen, K., Corrado, G., Dean, J.: Efficient estimation of word representations in vector space. In: Bengio, Y., LeCun, Y. (eds.) 1st International Conference on Learning Representations, ICLR 2013, Scottsdale, Arizona, USA, May 2-4, 2013, Workshop Track Proceedings (2013). <http://arxiv.org/abs/1301.3781>
- [19] Poličar, P.G., Stražar, M., Zupan, B.: Embedding to reference t-SNE space addresses batch effects in single-cell classification. *Machine Learning*, 1–20 (2021) <https://doi.org/10.1007/s10994-021-06043-1>